Cut-edge corrosion behavior assessment of newly developed environmental-friendly coating systems using the Scanning Vibrating Electrode Technique (SVET)

Sina Sheikholeslami [a,*], Geraint Williams [b], H. Neil McMurray [b], Louis Gommans [c], Scott Morrison [c], Sonny Ngo [d], David E. Williams [a], Wei Gao [a]

[a] *The University of Auckland, 5 Grafton Road, Auckland 1142, New Zealand*
[b] *Materials Research Centre, College of Engineering, Swansea University, United Kingdom*
[c] *Fletcher Steel Ltd, Penrose, Auckland, New Zealand*
[d] *Becker's Group, Liverpool, United Kingdom*
[*] *sshe933@aucklanduni.ac.nz , +1 416 895 8651*

Abstract

Accelerated cut-edge corrosion performance of commercialized full waterborne coating systems containing enviro-friendly corrosion inhibitors was studied on 55 wt.% Al, 44 wt.% Zn and 1 wt.% Si galvanized steel in 5 wt.% NaCl solution at ambient temperature via the Scanning Vibrating Electrode Technique (SVET). At the same volume content (7-11 wt.%), benzotriazole pigments had a better overall cut-edge corrosion performance than calcium ion exchanged silica pigments. It was due to benzotriazole's superior cathodic protection of the cut-edge in comparison with calcium silicate. Furthermore, although both enviro-friendly inhibitors did not exhibit the same performance level as the conventional Cr(VI)-containing system, they exhibited promising results in inhibiting cut-edge corrosion in a fully commercialized waterborne coating system.

Keywords

Galvanized steel, cut-edge, corrosion, SVET, benzotriazole, calcium silica, waterborne, environmental-friendly, coil coating

1. Introduction

Cut-edge corrosion in galvanized steel is a major failure in the coil-coating industry. It causes delamination of the organic layer and degradation of Zn accelerated by the unfavorable anode-to-cathode area ratio [1]. In natural NaCl solution conditions, the zinc/steel galvanic corrosion reaction is defined as Equations 1 and 2 [2].

$$Zn\ (s)\ \rightarrow\ Zn^{+2}\ (aq) + 2\ e^{-} \qquad Eq.(1)$$

$$O_2\ (g) + 2\ H_2O\ (l) + 4\ e^{-}\ \rightarrow\ 4\ OH^{-}\ (aq) \qquad Eq.(2)$$

The dissolved oxygen in the solution is reduced on the steel substrate at the cut-edge to form hydroxyl species. However, since the distance between the anodic and cathodic regions is very short at the cut-edge, chemical interactions and large concentration gradients of ionic species influence the corrosion process [2]. One example of these effects is the alkalization of the surrounding environment; the cut-edge would facilitate the precipitation of corrosion products on the steel rather than over the galvanized layer [3].

Zinc and strontium chromates have been the most effective corrosion inhibition pigment used in the coil-coating industry for many years [4-6]. Chromate species act as inhibitors due to the oxidizing power of Cr(VI) reducing to Cr(III) (according to Equation 3) and formation of a passive layer of chromium oxide. The passive layer covers the steel substrate and protects it from corrosion [7].

$$2\ CrO_4^{-2} +\ 5\ H_2O +\ 6\ e^{-} \rightarrow\ Cr_2O_3 +\ 10\ OH^{-} \qquad Eq.(3)$$

However, using chromate pigments has faced excessive restrictions worldwide due to environmental and health concerns. Calcium (Ca^{+2}) cations are considered a potential alternative non-toxic inhibitor to Cr(VI), and several inhibitor systems were developed based on them [8-14]. Shieldex® is a commercially available cation pigment technology made up of exchangeable calcium silica (SiO_2^{-}) [3, 15-18]. This inhibitor is typically prepared by treatment of SiO_2 powder with calcium hydroxide ($Ca(OH)_2$) [19]. Several studies showed that the corrosion protection of steel with Ca^{+2}-SiO pigments could be as good as using conventional chromate species in certain conditions [20, 21]. It is known that silicates form complex colloidal structures in an aqueous environment [22]. Therefore, their inhibition efficiency vastly depends on the pH and concentration of salt in the environment [23].

Previous studies concluded that Ca^{+2} ions derived from Ca-containing inhibitor pigments effectively enhance the cathodic protection of the coating system in NaCl solutions. The reaction of these ions with hydroxyl species will end up in the precipitation of passivated products on the alkaline cathodic

areas [2]. Silica releases calcium ions in exchange for cations such as H^+ or Na^+. Ca^{2+} reacts with silicate ions to form a calcium silicate film. Hence, leached Ca^{+2} ions together with polysilicate ions form a passive layer on the surface of the metal. The literature also suggests that parallel to the silicate ion reaction, silicate ions react with zinc ions and form zinc silicate at the anodic region. The zinc silicate and calcium silicate combined to form mixed zinc silicate and calcium silicate protective layer. [22-25].

Benzotriazole (BTA) has also been investigated as an organic corrosion inhibitor due to its reasonable solubility in aqueous solutions, low toxicity, and low cost [26, 27]. It is believed that benzotriazole is stable in several forms depending on the pH; neutral BTA at pH<8, deprotonated BTA^- ions at pH>8, and protonated BTA^{+2} ions at pH<2 [28, 29]. BTA and its derivatives are known to form a complex between the metal and inhibitor species that by nature is a passivated and protective layer. In Zn-containing alloy steel, it was observed that the corrosion resistance of the alloy improves by forming a mixed oxide/Zn(II)BTA complex. In such conditions, Zn(II)BTA reinforces the formed zincite (ZnO), and therefore, BTA is considered as a corrosion inhibitor for Zn species [30-34]. In galvanized steel, a BTA film is formed on both the galvanized layer and steel at the cut-edge, which anodically polarizes the galvanized layer and reduces the electrochemical activity [26].

The atmospheric performance of conventional galvanized coatings consisting of zinc with <0.2% aluminum, is poor; especially in a pollutant-containing atmosphere. Therefore, Zn-Al systems were developed and proven more effective in severe atmospheric conditions with a reduction in the galvanized layer [35-37]. It has been previously demonstrated that benzotriazole is an effective corrosion inhibitor in Zn-Al systems [38-40]. Organic pigments containing BTA protect the coil through exchanging the BTA anion as oppose to corrosive anions (such as Cl^-) and formation of Zn-Al LDH (layered double hydroxide) [41-43]. The positive effects of such BTA/layered double oxide pigments on Al and Zn have been reported by Richards et al. [44].

However, previous studies did not consider that the complexity of fully commercialized coating systems dramatically affects the inhibition performance. The media at which the inhibitors were doped and tested in these studies were either stock solutions or a single-layer organic matrix made up of PVB in previous approaches. In this study, though, full commercialized systems consisting of a substrate, galvanized coating, pre-treatment, primer, and topcoat were used instead. As a result, the corrosion behavior of full waterborne commercial systems doped with calcium silicate and BTA pigments were studied at the cut edge via the Scanning Vibrating Electrode Technique (SVET). The results were benchmarked against the performance of conventional solvent-based Cr(VI) system via

SVET to compare the effectiveness of our newly-developed enviro-friendly systems manufactured by Fletcher Steel Ltd and Becker's Group.

2. Materials and Methods

2.1. Materials

Commercialized coating systems were prepared by Fletcher Steel Ltd in Auckland, New Zealand. Designs were made to satisfy the wide range of roofing standards according to the Australia/New Zealand regional standards. A general overview of the systems is shown in Figure 1. The manufacturing process started with cleaning and activating the surface of the 0.7mm thick galvanized steel coil with 15-20 µm of Al-Zn galvanized coating on both sides. The galvanized layer composition was 55 wt.% Al, 44 wt.% Zn and 1 wt.% Si [45]. The primer was then applied and cured on top of the galvanized layer on both sides with 10-15 µm thickness.

Four different types of Chromate-Containing (CC) and Chromate-Free (CF) primers were applied individually and studied in this research, as summarized in Table 1. The CC-Cr(VI) system was the conventional solvent-based primer doped with Cr(VI)-containing inhibitor pigments. The other three were all newly-developed chromate-free waterborne primers with Ca(II) ion-exchange silica or benzotriazole inhibitors with different volume content. All chromate-free primers were developed in Becker's Group R&D center in the United Kingdom and batches were made in the Malaysia branch. A final waterborne topcoat with approximately 20 µm thickness was applied on top of all coating systems as the roofing industry requirement.

Table 1 - Primer systems specification manufactured in Fletcher Steel Ltd

Primer	Base	Inhibition system	Volume content (%)
CC - Cr	Solvent	Cr(VI)	controlled
CF - Ca	Waterborne	Ca(II) exchange silica	7-11
CF - BTA high	Waterborne	Benzotriazole	7-11
CF - BTA low	Waterborne	Benzotriazole	3.5-5.5

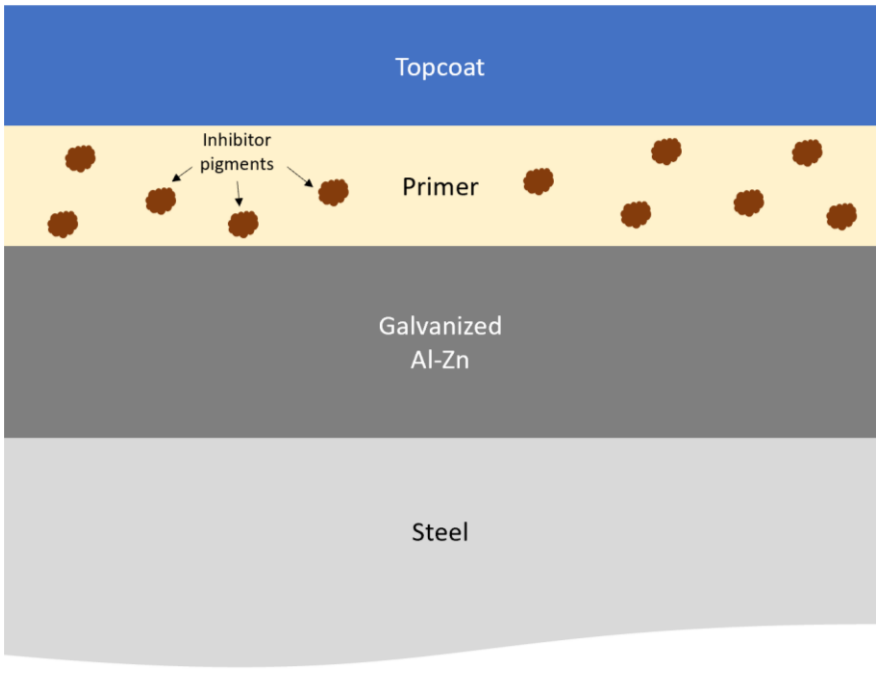

Figure 1 - Schematic cross-sectional view of the commercialized coating systems manufactured by Fletcher Steel Ltd

2.2. Methods

Several 10×10 mm specimens were cut out of coated panels with a guillotine cutter. The specimens were mounted in non-conductive epoxy in a way to expose the cut edge only. Thickness of the mounted specimens was 15mm. Mounted samples were then ground with grid #400 to #1200 silicon carbide abrasive papers and polished with 9, 3, and 1 µm water-based diamond suspensions, respectively, to achieve a smooth surface at the cut edge as required by the SVET. Specimens were individually fastened at the bottom of a glass dish, and 250 ml of 5 wt.% NaCl in deionized water solution were poured into the dish as the accelerated corroding media in ambient temperature.

General information regarding the SVET setup and calibration steps is found in the literature [46-52]. In summary, a 125µm-thick Pt microtip covered in glass vibrates at the fixed frequency of 140 Hz in the *Z* direction, meaning that the probe only vibrated vertically. But scaning directions was through the X and Y axis horizontally, covering the surface of the specimen. The thickness of the probe body was 250 µm. The wire is sealed in the glass so that the probe tip consistently remains the only active site. The scanning height was set to 150 µm with vibration amplitude of 30 ±5 µm for all tests to ensure that the tip picks up strong signals without dragging any corrosion product deposited on top of the system throughout the test. the SVET voltage signal was detected using a lock-in

amplifier (Perkin Elmer 7265). The scanning box was a 2×11 mm rectangle with 100 µm resolution to cover the cut-edge completely. The SVET device was programmed to run one full scan per hour for the total duration of 24 hours, resulting in 24 full scans of the cut-edge per specimen. At least two samples per each coating system were tested via the SVET to ensure the data's reliability.

Quantification of localized corrosion rate was obtained by numerical integration of SVET-derived current density distributions, which provides a value of integrated anodic and cathodic currents (i_a and i_c, respectively) emerging from the exposed surface for each individual scan. By summing the area-averaged anodic current density values throughout the experiment to obtain a total anodic current (I_a), a total equivalent mass loss can be calculated by applying Faraday's relation as indicated in Equation 4 [45].

$$Mass\ loss = \frac{I_a \times t \times Ar_{element}}{n \times F} \qquad Eq.(4)$$

Where I_a is the sum of total anodic current emerging over the entire experiment, t is the time-lapse interval duration, $Ar_{element}$ is the molar mass of the corroding element, n is the number of the exchanged electrons in the anodic reaction of the element, and F is the Faraday constant that is 96,500 C/mol.

3. Results and discussion

Figure 2 shows the sum of anodic current density via the SVET from the specimens after 24 hours of submersion in 5 wt.% NaCl. The CC-Cr specimen had a relatively low sum of anodic current density during the test compared to the Cr-free specimens. The CF-BTA high specimen's anodic current density was approximately 25% lower than the CF-BTA low sample. Therefore, the volume content of benzotriazole pigments in the former system was more effective than the latter in Zn corrosion inhibition. Also, benzotriazole pigments were slightly more effective than calcium silica pigments with the same volume content according to their results. The total mass loss of these specimens calculated via the SVET test can be found in

Table 2. Correspondingly, the CC-Cr specimen had lower mass loss than the other systems with 34 mg in 24 hours. The Cr-free Ca, BTA high, and BTA low specimens had 40, 37, and 48 mg total mass loss, respectively. These results suggested that the Cr-containing primer had better corrosion

performance at the cut-edge in submerged NaCl conditions overall. The CC-Cr primer was 10% better than the 2nd best primer (CF-BTA high), and 30% better than the worst primer (CF-BTA low) regarding the total mass loss.

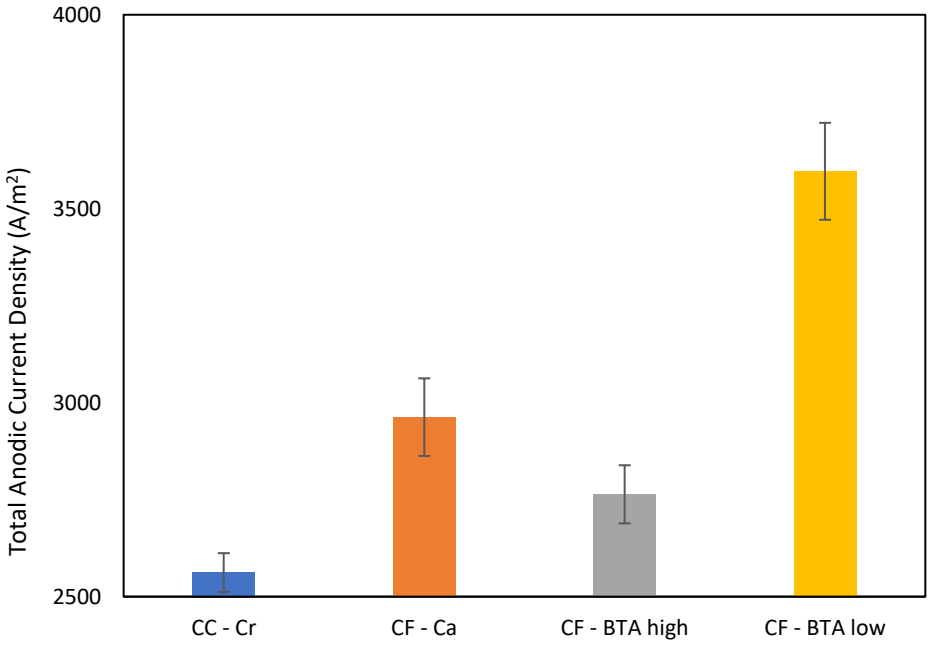

Figure 2 - Total anodic current density of different coating systems after 24 hours in 5 wt.% NaCl solution via SVET

Table 2 - Total mass loss of coating systems after 24 hours in 5 wt.% NaCl solution via SVET

Specimen	Total loss (mg)
CC-Cr	34
CF-Ca	40
CF-BTA high	37
CF-BTA low	48

Figure 3 illustrates a time-lapse view of the total anodic current density of coating systems at the cut-edge during 24 hours in 5 wt.% NaCl solution for each scan via the SVET. The difference between the Cr-containing and Cr-free systems can easily be seen in this figure. The anodic current density per hour for the CC-Cr(VI) system started increasing from 88 to 126 A/m^2 during the first 12 hours and then decreased back to 88 A/m^2 with a steady trend overall. On the other hand, the Cr-free systems started with a relatively high anodic current density than the CC-Cr(VI) system and continuously decreased during the test. The CF-BTA high system had a continually lower anodic current density

value through the test among all Cr-free primers. The CF-Ca system was the 2nd best Cr-free primer, standing between the CF-BTA high and low systems at all times.

The anodic current density for CC-Cr, CF-Ca and CF-BTA high in the end came down to approximately 90 A/m^2 (with a slightly lower value for CC-Cr at 88 A/m^2). This showed that with a controlled amount of corrosion inhibitors in a real coating system, a relatively small exposed cut-edge would mostly be passivated by corrosion products after 24 hours of immersion in 5 wt.% NaCl solution to the same extend. However, not only The CF-BTA low primer exhinited constantly higher anodic current density, it was also not able to pacify the anodic reaction to the same level as other corrosion inhibitors after 24 hours.

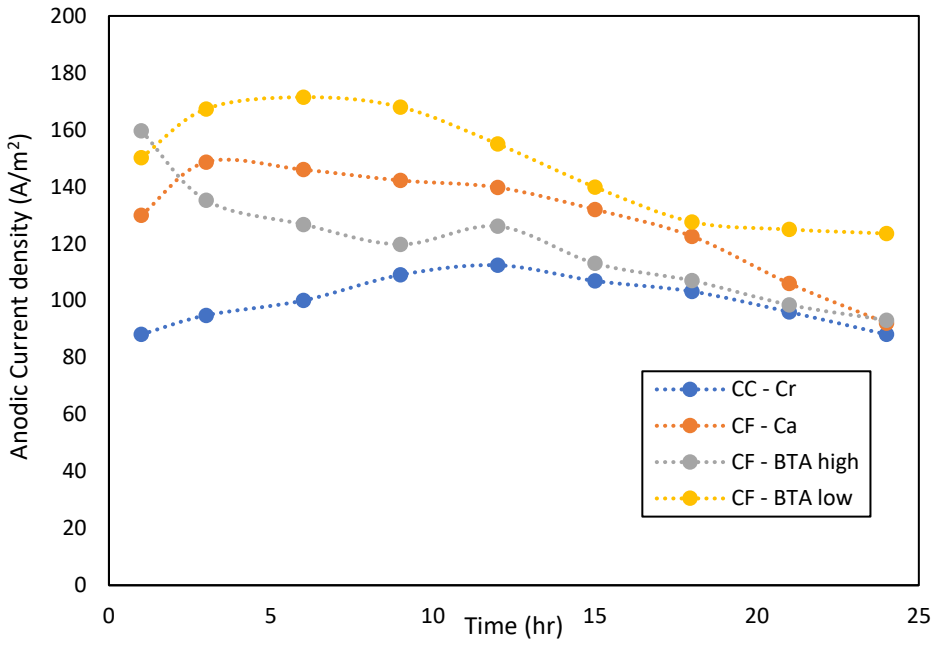

Figure 3 – Time-lapse view of the total anodic current density changes of different coating systems during 24 hours in 5 wt.% NaCl solution for each scan via SVET

Figure 4 to Figure 7 illustrate 2D current density maps by SVET of the CC-Cr(VI), CF-Ca, CF-BTA high, and CF-BTA low systems in 5 wt.% NaCl solution after several immersion times. Red and blue areas are active anodic and cathodic regions, respectively. The colour lightness in these maps indicates the severity of either localized anodic or cathodic reactions. The position of the galvanized specimens are approximately illustrated with a box in Figure 5. These current density maps facilitate the comparison of anodic current intensity, anodic region size, and distribution at the cut-edge of

these coating systems. As expected, the steel substarte was being cathodically protected by the sacrificial localized anodic reaction on galvanized layer according to the maps.

The anodic corrosion reaction was pacified overtime for all systems at the cut-edge. The anodic current density in active anodic regions decreased compared to previous scans' value. In addition, the maps indicated that the anodic reaction intensity in all Cr-free specimens was higher compared to the CC-Cr(VI) system (Figure 4-A to Figure 7-A). The corrosion reaction seemed to be more active at the cut-edge of the CF-Ca specimen (Figure 4-B to Figure 7-B) compared to the CF-BTA high specimen (Figure 4-C to Figure 7-C); the anodic current density for the CF-Ca system was noticeably higher.

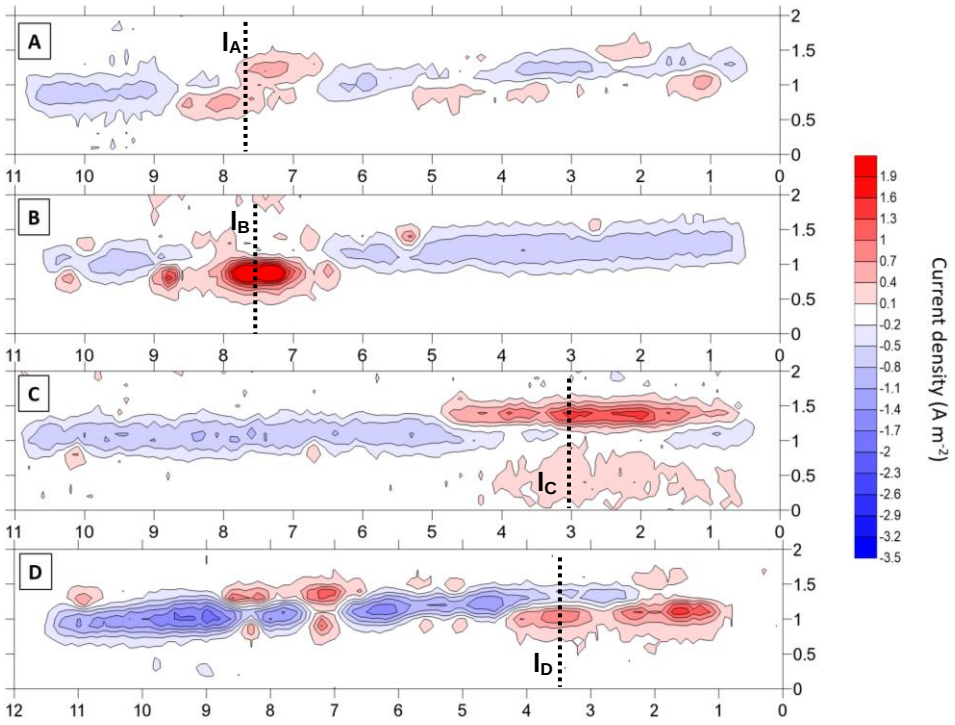

Figure 4 - SVET 2D current density maps after 1 hour in 5 wt.% NaCl solution: A) CC - Cr, B) CF - Ca, C) CF - BTA High, and D) CF - BTA low

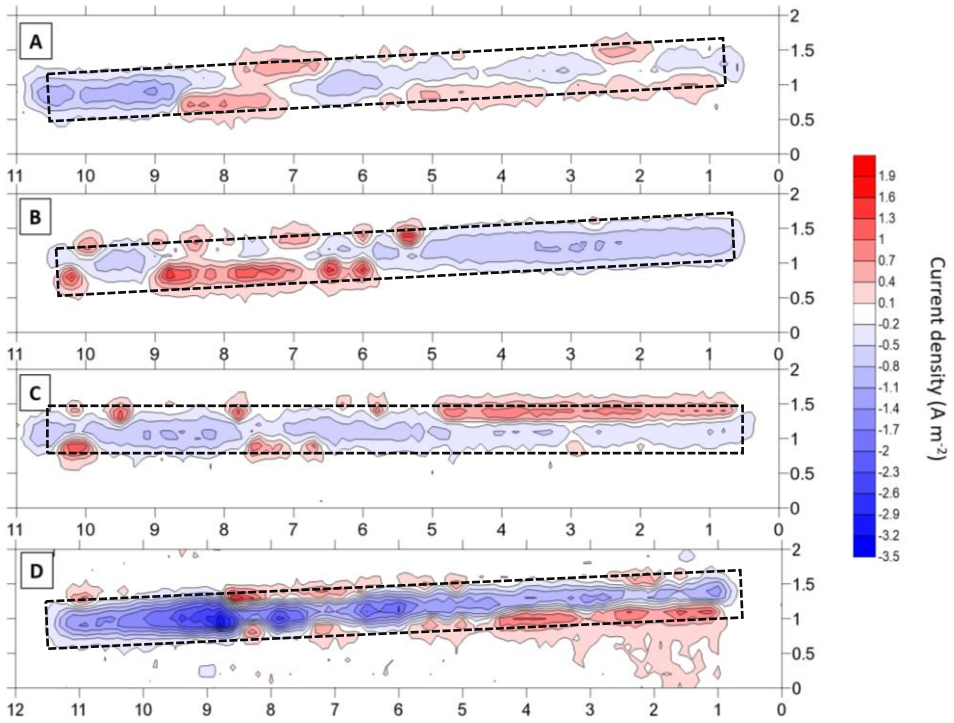

Figure 5 - SVET 2D current density maps after 6 hours in 5 wt.% NaCl solution: A) CC - Cr, B) CF - Ca, C) CF - BTA High, and D) CF - BTA low

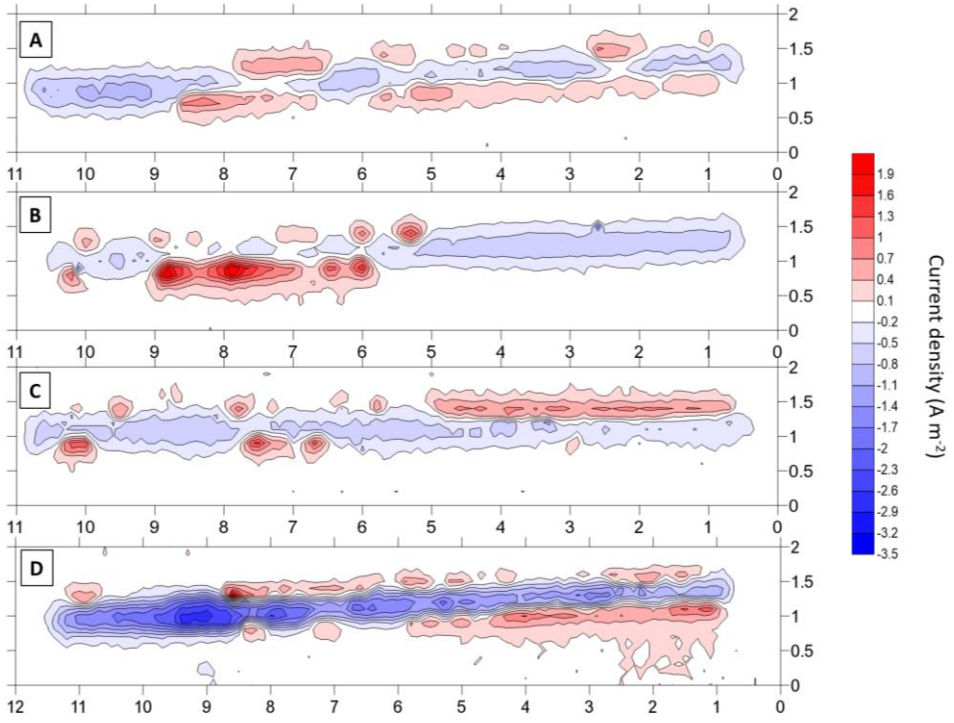

Figure 6 - SVET 2D current density maps after 12 hours in 5 wt.% NaCl solution: A) CC - Cr, B) CF - Ca, C) CF - BTA High, and D) CF - BTA low

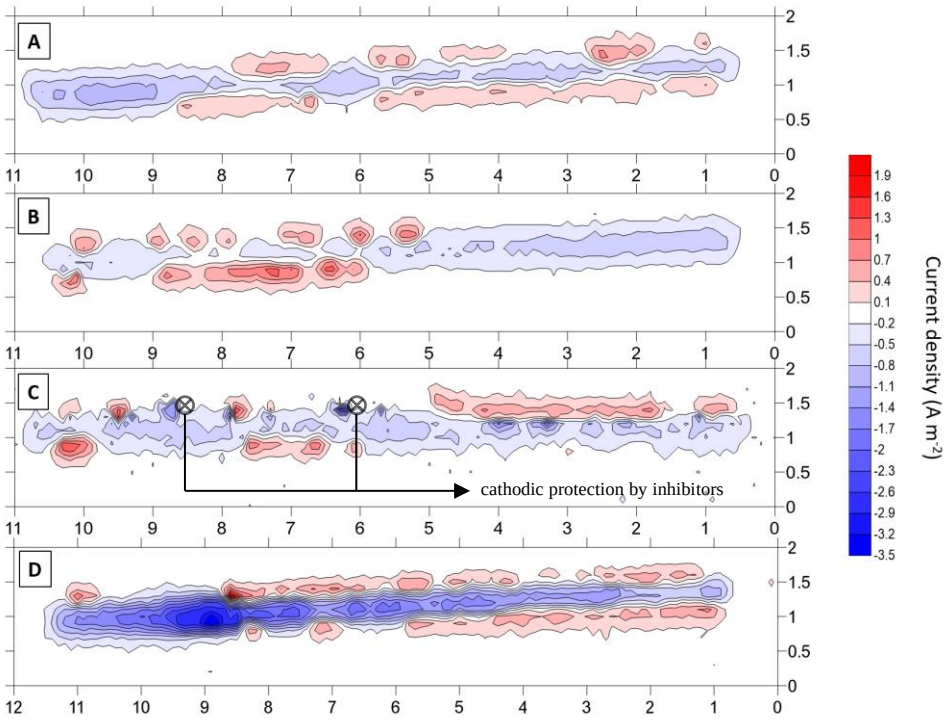

Figure 7 - SVET 2D current density maps after 24 hours in 5 wt.% NaCl solution: A) CC - Cr, B) CF - Ca, C) CF - BTA High, and D) CF - BTA low

Moreover, the effect of inhibition systems on the cathodic reaction can also be investigated by looking at the current density maps in Figure 4 to Figure 7. According to the maps, the cathodic reaction mostly occurred in the middle of the cut-edge on the entire exposed steel substrate. Same results with regards to anodic and cathodic activtity has been reported in other studies as well [2, 53, 54]. It was due to the galvanic coupling of Fe and Zn, resulting in the reduction of O_2 as shown in Equation 2 on the surface of exposed steel, and releasing OH^- species [2]. Some cathodic activities occurred on the top of the galvanized layer where no anodic behavior was observed, as shown in Figure 7-C. It can be attributed to the cathodic protection of the galvanized coating by passivated corrosion products from inhibitors at lower pH. Such capability of BTA in cathodically inhibiting the galvanized layer as well as the steel substrate has been previously reported as shown in Equation 5, where M is a transition metal [26, 44]. However, the intensity of cathodic current density on the steel was higher than in these areas. Additionally, it is hard to pick up cathodic current density from the cathodic protection of inhibitor pigments due to the SVET limits and the pH value was not measured during the SVET test. Therefore, it was assumed that all cathodic current density values belong to the O_2 reduction reaction.

$$(MBTA)_n + n\,H^+ + n\,e^- \rightleftharpoons nM + nBTA \qquad Eq.(5)$$

The literature suggests that due to increasing pH and the presence of inhibitive species, a passive layer is formed on top of the surface of exposed steel at the cut-edge. This layer shields the steel surface and, more importantly, isolates it from the corrosive media. As a result, smaller areas prone to host the cathodic reaction will exist over time. This reduces the cathodic activity on the substrate and eventually inhibits the corrosion reaction. Figure 8 illustrates the maximum cathodic current density picked up by the SVET during the test from the coating systems. The CC-Cr(VI), CF-Ca, and CF-BTA high specimens efficiently maintained the maximum cathodic current density at relatively low levels through the SVET test. The intensity of their maximum cathodic current density was significantly lower than the CF-BTA low system ay every point during the test.

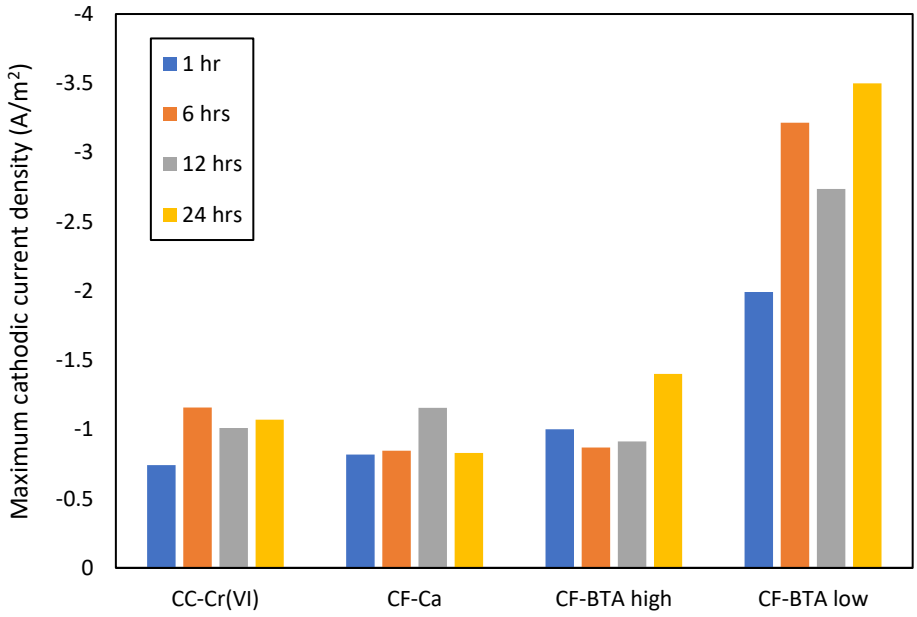

Figure 8 - Maximum cathodic current density picked up by the SVET for coating systems submerged in 5 wt.% NaCl solution

Figure 4-D to Figure 7-D also visually show that the cathodic activity on the steel in the CF-BTA low system was higher than the rest of the specimens. Since the volume content of corrosion inhibitors in the CF-BTA low system was lower than the others, it was concluded that the inhibition system in this primer was not capable enough to deposit a uniform passivated layer on the exposed steel. Therefore, this primer was not able to cathodically inhibit the corrosion reaction as well as the others. Based on this analysis, the optimum volume content of benzotriazole required to inhibit the cathodic corrosion reaction effectively was between 7-11%.

Figure 9 shows the analysis of anodic area size per total scanned area at the cut-edge during the 24-hour testing in 5 wt.% NaCl solution by SVET. Each SVET scan covered a 2×11mm area, while SVET probe recorded a current density reading every 100μm as it continued scanning the surface. Therefore, each scan result consisted of 20×110 current density readings, mapping the whole cut-edge and parts of the mount. The anodic area analysis was calculated based on the number of positive recorded readings divided by total number of readings (excluding readings that were approximately 0 A/m^2 which were picked up from electrochemically inactive areas on the mount).

The overall trend for CF-BTA high was generally downward, showing that the anodic areas became smaller over time. In contrast, CF-Ca started from a relatively small anodic area, gradually increased for up to 9 hours, and then steadily decrease until the end. The CC-Cr system also exhibited the same trend as CF-Ca, with the only exception that its anodic area was decreasing for up to 12 hours, before it started to steadily decline. This observation indicated that there is a fundamental difference between anodic inhibition of CF-BTA with CF-Ca or CC-Cr. Ranking according to the anodic area size per scanned area was not necessarily an estimation of better overall cut-edge corrosion performance. additionally, the correlation between anodic area size changes over time and the integral values of current density can be used to indicate if anodic corrosion inhibition was being effectively in progress, and if yes, for how long. One of the possible reasons for expantion of anodic area is that localized anodic activity was affected by an anodic inhibition reaction and it had to expand to generate enough anodic activity to continue with the corrosion process. However, if the anodic site was corroding without inhibition disturbance, then it would not expand to maintain the small distance between anodic and cathode. Since anodic activity tend to occur locally for CF-BTA during the first 12 hours, it can be said Zinc Silicate was more effective in passivating anodic areas compared to reinforced $ZnO/Zn(BTA)_2$.

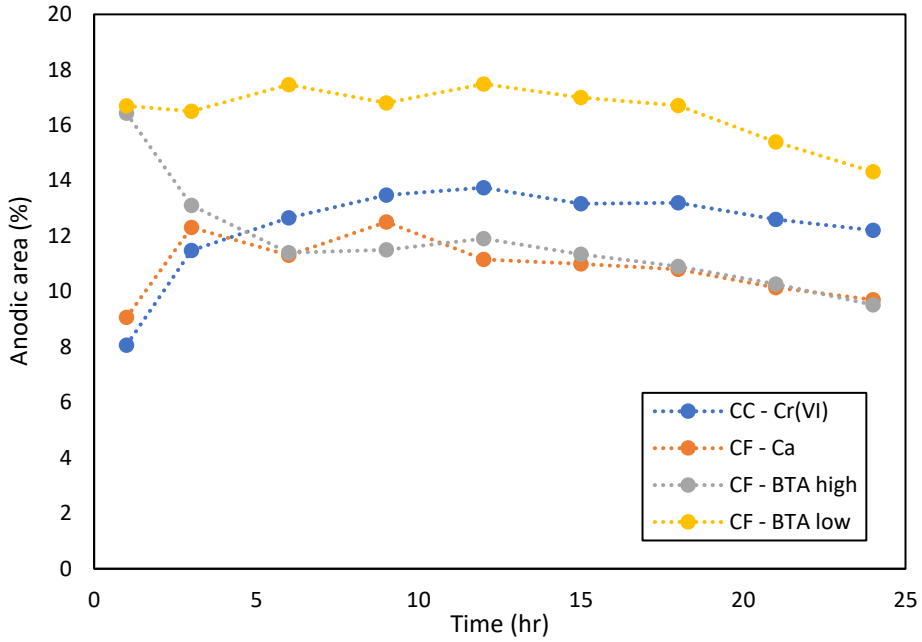

Figure 9 - Anodic area size analysis per total scanned area at the cut-edge during the 24-hour testing period by SVET

The chromate-free systems showed higher anodic current density than the CC-Cr(VI) system. They also exhibited a potential delay in effectively inhibiting the anodic reaction with a decreasing trend in downsizing the anodic areas at the cut-edge. Among the chromate-free systems, the CF-BTA high system demonstrated better corrosion performance than the others; because it had a relatively lower mass loss at the cut-edge and smaller anodic areas. The CF-Ca system was less effective than the CF-BTA high due to its higher mass loss, although the size and distribution of the anodic regions in both systems were almost the same. The CF-BTA low specimen was the least corrosion-resistant system because of its high mass-loss/total anodic current density and large anodic areas. Therefore, ranking these systems in terms of corrosion performance and mass loss at the cut-edge submerged in 5 wt.% NaCl solution via the SVET resulted in CC-Cr(VI) > CF-BTA high > CF-Ca > CF-BTA low.

The reason for such behavior seemed to be better cathodic protection performance of BTA compared with Ca/Ca^{+2} and Silica pigments at the cut-edge. In a parallel research to this study, we concluded that Shieldex can be more protective than Benzotriazole with regards to pacifying anodic corrosion reaction [45]. However, it is more important that the exposed steel is uniformly and effectively passivated when the size of cathodic region is relatively large. Current density mapping showed that the CF-Ca sample had larger and more intense cathodic activity on its exposed steel compared to CF-BTA high. The cathodic inhibition mechanisms of benzotriazole and calcium silicate on exposed galvanized steel have been studied and reported earlier [19, 20, 44]. Therefore, it can be concluded

that passivated benzotriazole products can more uniformely protect the exposed steel against cathodic reaction compared to passivated calcium silicate, and Ca/Ca^{+2} exchange mechanism with Na^{+} and H^{+} is not as effective as passivation of BTA^{+}.

To study the effect of each inhibition system on the anodic Zn/Zn^{+2} reaction, Figure 10 plots changes of anodic current density over time in the lines drawn in Figure 4. These lines (l_A in the CC-Cr(VI), l_B in the CF-Ca, l_C in the CF-BTA high, and l_D in the CF-BTA low systems) were selected where the maximum change in the anodic current density values occurred in each coating system. In Figure 10-A, the anodic current density of the CC-Cr(VI) system was at its lowest for the first hour and increased over time. However, the maximum current density value in this specimen (which occurred at the 12^{th} scan) was lower than the maximum current density compared to the other samples. It indicates that the conventional Cr-containing system showed superior corrosion performance than the others by illustrating more controlled changes in its anodic current density value. For all Cr-free systems, the anodic current density gradually decreased over time.

Changes in the cathodic behavior on exposed steel were almost similar in all specimens regardless of their inhibition system. The cathodic current density continuously increased in all systems. While the CF-Ca and CF-BTA high systems did not demonstrate a minimum cathodic current lower than -0.8 A/m^2 (Figure 10-B and Figure 10-C), the CF-BTA low system recorded -1.2 A/m^2 for its 12^{th} and 24^{th} scan according to Figure 10-D. The linear current density analysis also concluded that the cathodic reaction occurred without effective inhibition at the cut-edge of the CF-BTA low system.

The maximum anodic current density and its rate of change were recorded and calculated based on Figure 10 and were plotted in Figure 11. The CC-Cr(VI) system showed moderate fluctuations, starting from 0.4 A/m^2 and ending at 0.3 A/m^2. On the other hand, the Cr-free systems showed a downward trend with their maximum anodic current density over time. The CF-Ca system recorded 2.8 A/m^2 for the first scan and ended up with 1 A/m^2 during the final scan. The maximum current density per scan in the CF-BTA high and low systems also declined from 1.4 A/m^2 to 0.5 A/m^2 and 1 A/m^2 to 0.6 A/m^2, respectively.

Additionally, a statistical analysis based on the difference between the initial and final value of the maximum anodic current density divided by the initial value was used to compare the data. This analysis showed that the anodic current density reduction in the CF-Ca and Ca-BTA high systems were both equal to 65%. However, the CF-BTA low system had only a 40% reduction, indicating that this system was approximately 25% less effective than the other Cr-free samples. The anodic inhibition efficiency based on the maximum anodic current decrease was equal in the CF-Ca and CF-

BTA high systems and better than the CF-BTA low specimen. Therefore, the performance difference was caused by the volume content of corrosion inhibitors in the system.

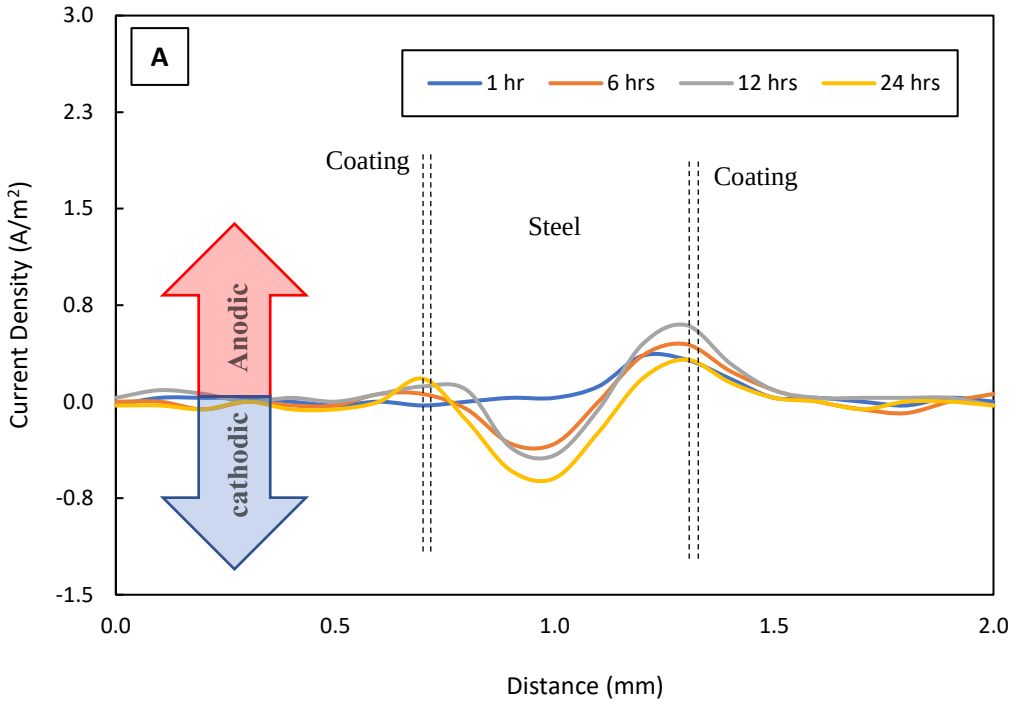

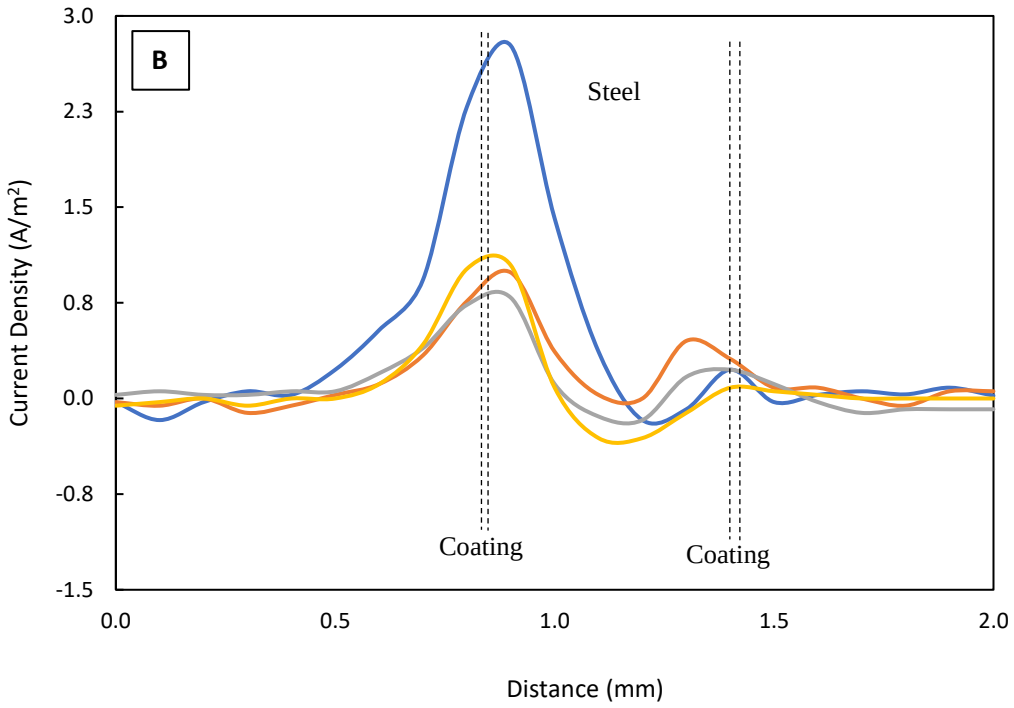

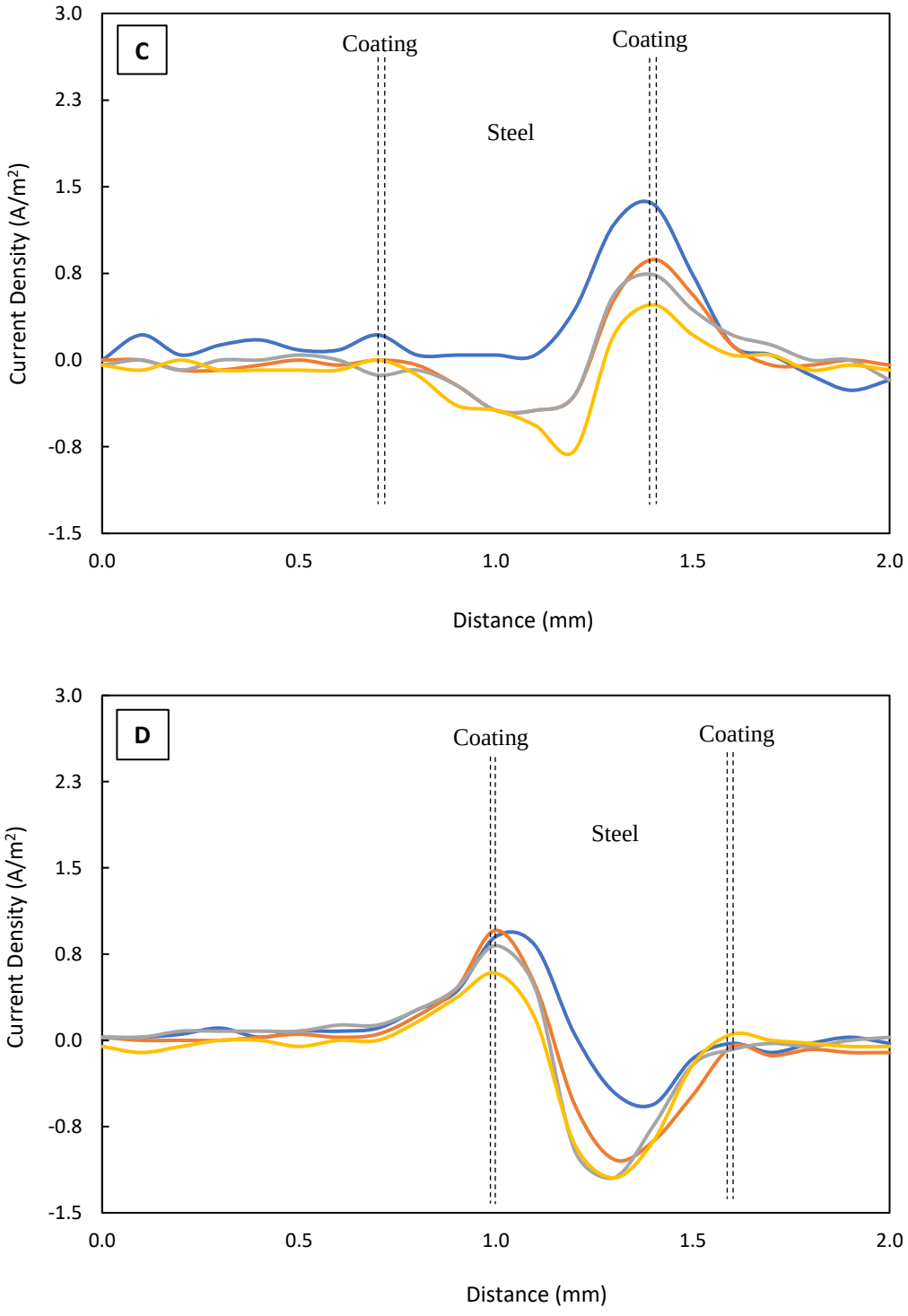

Figure 10 - Linear current density time-lapse for different coating systems: A) l_A in CC-Cr(VI), B) l_B in CF-Ca, C) l_C in CF-BTA high, and D) l_D in CF-BTA low

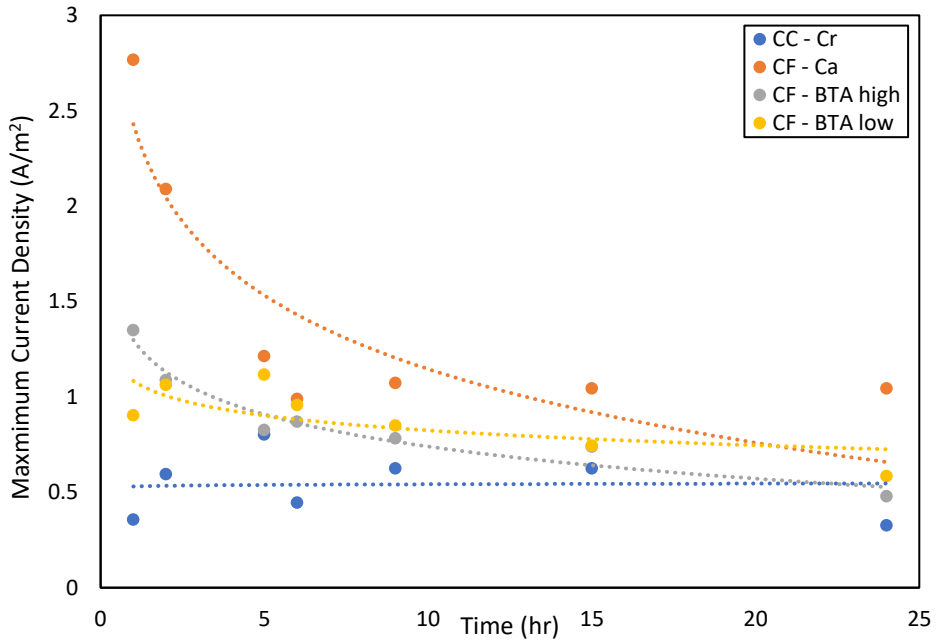

Figure 11 - Maximum anodic current density in linear scan for different coating systems

The anodic current density rate of change was calculated as δ(current density)/dt per specimen, and was plotted in Figure 12 to understand the effect of the Ca/Ca^{+2} and BTA species on anodic corrosion reduction at the cut-edge of the system. The CC-Cr(VI) system showed a steady-state trend through the test. In contrast, all Cr-free systems started from higher changing rates and eventually came to a lower steady pace in the end. The Ca^{+2} ion exchange system, known as Shieldex®, showed a relatively high changing ratio in the maximum anodic current density per scan than other Cr-free systems. Also, the rate of change was the same in the CF-BTA high and low systems (with a negligible difference due to the SVET error), despite their volume content difference. This behavior confirmed results from our parallel investigation regarding anodic inhibition capabilities of Shieldex and Benzotrizole pigments [45]. As mentioned in the literature, SiO_3^{-2} ions emerged from silica pigments react with Zn^{+2} ions on top of galvanized layer and form zinc silicate, which passivates the galvanized layer [2]. Deprotonated benzotriazole, on the other hand, reacts with Zn^{+2} and forms reiforced ZnO with $Zn(BTA)_2$ and passivates the galvanized layer accordingly [44]. Based on the anodic inhibition mechanisms of these two pigments, it can be concluded that reinfoced ZnO/ $Zn(BTA)_2$ products may not necessarily be as uniform and protective as zinc silicate. Therefore, the Ca^{+2} ion exchange system would be a more effective inhibition system than BTA only when the anodic inhibition is considered.

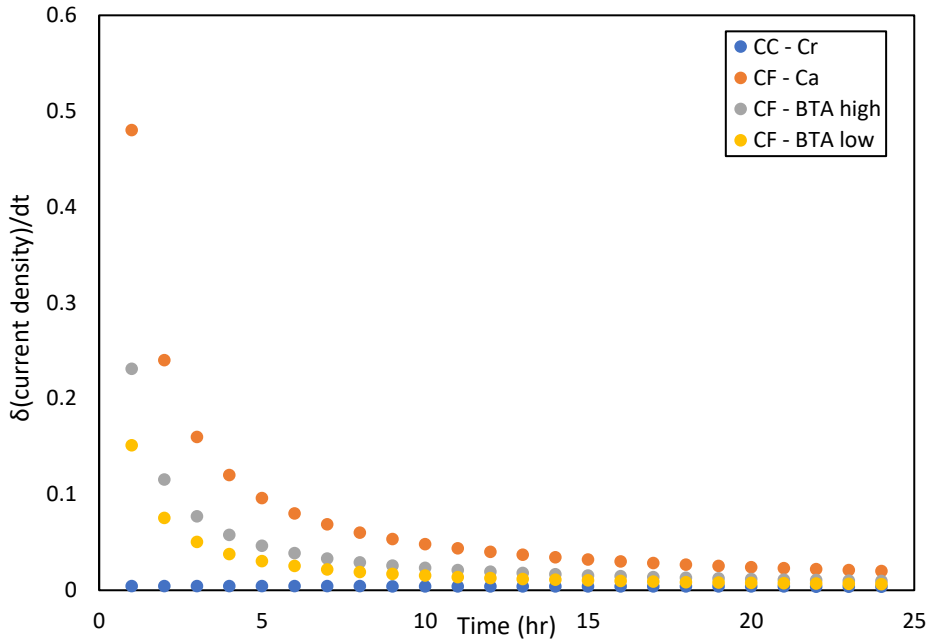

Figure 12 - Anodic current density changing rate over time for different coating systems

4. Conclusions

- Three newly developed full-waterborne commercialized coil coating systems on Al-Zn substrate were investigated for accelerated cut-edge corrosion assessment via the SVET and benchmarked against the conventional solvent-based Cr-containing system. It was found that the organic benzotriazole-containing system has superior corrosion protection than the Ca^{+2} ion-exchange silica system. With the same volume content of inhibitor pigments, the CF-BTA high system illustrated lower anodic current density and lower mass loss in 24 hours via the SVET at the cut-edge while submerged in 5 wt.% NaCl solution. The reason for this behavior is related to the superior ability of BTA species to uniformely passivate cathodic areas compared with calcium silica.

- The CF-BTA high system with higher volume content of BTA (7-11%) performed better than the CF-BTA low system 3.5-5.5% of BTA at the cut-edge. Based on this study and the results from previous studies, optimum volume content of benzotriazole in the current testing conditions was between 7-11%. Cut-edge corrosion in the CF-BTA low specimen was more intense since the value of cathodic current density on the surface of this specimen was much higher than the other primers. The results showed that the cathodic reaction occurred easily due to not enough inhibitor ion formed on the surface of the substrate and the passivated layer is non uniform.

- The conventional solvent-based chromate CC-Cr(VI) coating system was still the best regarding cut-edge corrosion performance compared to all waterborne chromate-free systems. However, the difference between the CC-Cr(VI) and CF-BTA high or CF-Ca systems via the SVET was surprisingly close. Therefore, the newly developed full-waterborne coating systems demonstrated promising cut-edge corrosion performance, considering that the systems were chromate-free and waterborne.

Acknowledgement

This study was sponsored by Fletcher Steel, Callaghan Innovation (a New Zealand Government Organization) and Uniservices. The authors wish to thank the executive boards at Fletcher Steel Ltd (New Zealand) and Becker's Group (United Kingdom and Malaysia), Dr. Chris Lowe, and Ms. Michelle Teo for their support. We also wish to pass our most sincere regards to the personnel and postgraduate students at the University of Auckland, and Swansea University for the help regarding the experimental work.

References

1. J. Elvins, J. A. Spittle, D. A.Worsley, *Microstructural changes in zinc aluminium alloy galvanising as a function of processing parameters and their influence on corrosion.* Corrosion Science, 2005. **47**(11): p. 2740-2759.
2. A. M. Simões, J. C. S. Fernandes, *Studying phosphate corrosion inhibition at the cut edge of coil coated galvanized steel using the SVET and EIS.* Progress in Organic Coatings, 2010. **69**(2): p. 219-224.
3. I. M. Zin, S. B. Lyon, V. I. Pokhmurskii, *Corrosion control of galvanized steel using a phosphate/calcium ion inhibitor mixture.* Corrosion Science, 2003. **45**(4): p. 777-788.
4. Z. L. Long, Y. C. Zhou, L. Xiao, *Characterization of black chromate conversion coating on the electrodeposited zinc–iron alloy.* Applied Surface Science, 2003. **218**(1-4): p. 124-137.
5. H. S. Isaacs, S. Virtanen, M. P. Ryan, P. Schmuki, L. J. Oblonsky, *Incorporation of Cr in the passive film on Fe from chromate solutions.* Electrochimica Acta, 2002. **47**(19): p. 3127-3130.
6. A. Amirudin, C. Barreau, R. Hellouin, D. Thierry, *Evaluation of anti-corrosive pigments by pigment extract studies, atmospheric exposure and electrochemical impedance spectroscopy.* Progress in Organic Coatings, 1995. **25**(4): p. 339-355.
7. A. C. Bastos, M. G. Ferreira, A. M. Simões, *Corrosion Inhibition by Chromate and Phosphate Extracts for Iron Substrates Studied by EIS and SVET.* Corrosion Science, 2006. **48**: p. 1500-1512.
8. F. Tedjar, J. Guitton, *The influence of the calcium-ion in saline electrode-electrolyte Interfaces, 1 Zinc corrosion.* Surface Technology, 1984. **23**(1): p. 83-90.

9. X. Jiang, Y. G. Zheng, D. R. Qu, W. Ke, *Effect of calcium ions on pitting corrosion and inhibition performance in CO2 corrosion of N80 steel.* Corrosion Science, 2006. **48**: p. 3091-3108.
10. A. A. Aghzzaf, B. Rhouta, E. Rocca, A. Khalil, J. Steinmetz, *Corrosion inhibition of zinc by calcium exchanged beidellite clay mineral: A new smart corrosion inhibitor.* Corrosion Science, 2014. **80**: p. 46-52.
11. B. Ramezanzadeh, E. Ghasemi, F. Askari, M. Mahdavian, *Synthesis and characterization of a new generation of inhibitive pigment based on zinc acetate/benzotriazole: Solution phase and coating phase studies.* Dyes and Pigments, 2015. **122**: p. 331-345.
12. R. Berger, U. Bexell, T. Mikael Grehk, S. E. Hörnström, *A comparative study of the corrosion protective properties of chromium and chromium free passivation methods.* Surface and Coatings Technology, 2007. **202**(2): p. 391-397.
13. G. Williams, H.N. McMurray, D.A. Worsley, *Cerium (III) inhibition of corrosion driven organic coating delamination studied using a scanning Kelvin probe technique.* Journal of Electrochemical Society, 2002. **149**: p. B154-B162.
14. S. E. Karekar, U. D. Bagale, S. H. Sonawane, B. A. Bhanvase, D. V. Pinjari, *A smart coating established with encapsulation of Zinc Molybdate centred nanocontainer for active corrosion protection of mild steel: release kinetics of corrosion inhibitor.* Composite Interfaces, 2018. **25**(9): p. 785-808.
15. L. W. Vasconcelos, I. C. P. Margarit, O. R. Mattos, F. L. Fragata, A. S. B. Sombra, *Inhibitory properties of calcium exchanged silica epoxy paintings.* Corrosion Science, 2001. **43**: p. 2291-2303.
16. F. Deflorian, I. Felhosi, *Electrochemical impedance study of environmentally friendly pigments in organic coatings.* Corrosion, 2003. **59**: p. 112-120.
17. M. Zubielewicz, W. Gnot, *Mechanisms of non-toxic anticorrosive pigments in organic waterborne coatings.* Progress in Organic Coatings, 2004. **49**(4): p. 358-371.
18. I. M. Zin, S. B. Lyon, L. M. Bilyi, M. B. Tymus, *Specific features of the corrosion inhibition of an aluminium alloy by a nonchromate pigment mixture.* Materials Science, 2008. **44**: p. 638-645.
19. G. Williams, S. Geary, H. N. McMurray, *Smart release corrosion inhibitor pigments based on organic ion-exchange resins.* Corrosion Science, 2012. **57**: p. 139-147.
20. N. Granizo, J. M. Vega, I. Díaz, B. Chico, D. de la Fuente, M. Morcillo, *Paint systems formulated with ion-exchange pigments applied on carbon steel: effect of surface preparation.* Progress in Organic Coatings, 2011. **70**: p. 394-400.
21. B. Chico, J. Simancas, J.M. Vega, N. Granizo, I. Dıaz, D. de la Fuente, M. Morcillo, *Anticorrosive behaviour of alkyd paints formulated with ion-exchange pigments.* Progress in Organic Coatings, 2008. **61**: p. 283-290.
22. M. Ebrahimi, T. Shahrabi, M. G. Hosseini, *Determination of suitable corrosion inhibitor formulation for a potable water supply.* Anti-corrosion Methods and Materials, 2004. **51**(6): p. 399-405.
23. M. Meeusen, L. Zardet, A. M. Homborg, M. Lekka, F. Andreatta, L. Fedrizzi, B. Boelen, J. M. C. Mol, H. Terrynae, *The effect of time evolution and timing of the electrochemical data recording of corrosion inhibitor protection of hot-dip galvanized steel.* Corrosion Science, 2020. **173**: p. 108780.
24. R. Romagnoli, M. C. Dey, B. del Amo *The mechanism of the anticorrosive action of calcium-exchanged silica.* Surface Coatings International Part B: Coatings Transactions, 2003. **86**: p. 135-141.
25. N. Granizo, M. I. Martín, F. A. López, J. M. Vega, D. De La Fuente, M. Morcillo, *Chemical and structural changes of calcium ion exchange silica pigment in 0.5M NaCl and 0.5M Na2SO4 solutions.* Afinidad, 2011. **68**(556): p. 439-446.

26. J. V. Custódio, S. M. L. Agostinho, A. M. P. Simões, *Electrochemistry and surface analysis of the effect of benzotriazole on the cut edge corrosion of galvanized steel.* Electrochimica Acta, 2010. **55**(20): p. 5523-5531.
27. I. Briguglio, S. Piras, P. Corona, E. Gavini, M. Nieddu, G. Boatto, A. Carta, *Benzotriazole: An overview on its versatile biological behavior.* European Journal of Medicinal Chemistry, 2015. **97**: p. 612-648.
28. J. Rodriguez, M. Mouanga, A. Roobroeck, D. Cossement, A. Mirisola, M. G. Oliviera, *Study of the inhibition ability of benzotriazole on the Zn-Mg coated steel corrosion in chloride electrolyte.* Corrosion Science, 2018. **132**: p. 56-67.
29. M. Finšgar, I. Milošev, *Inhibition of copper corrosion by 1,2,3-benzotriazole: a review.* Corrosion Science, 2010. **52**(9): p. 2737-2749.
30. A. M. Fenelon, C. B. Breslin, *An electrochemical study of the formation of Benzotriazole surface films on copper, zinc and copper-zinc alloys.* Journal of Applied Electrochemistry, 2001. **31**: p. 509-516.
31. T. Kosec, D. Kek Merl, I. Milošev, *Impedance and XPS study of benzotriazole films formed on copper, copper–zinc alloys and zinc in chloride solution.* Corrosion Science, 2008. **50**(7): p. 1987-1997.
32. K. Aramaki, *Effects of organic inhibitors on corrosion of zinc in an aerated 0.5 M NaCl solution.* Corrosion Science, 2001. **43**: p. 1985-2000.
33. S. Liu, Y. Zhong, R. Jiang, Z. Zeng, Z. Feng, R. Xiao, *Corrosion inhibition of zinc in tetra-n-butylammonium bromide aerated aqueous solution by benzotriazole and Na3PO4.* Corrosion Science, 2011. **53**: p. 746-759.
34. K. Wang, H.W. Pickering, K.G. Weil, *Corrosion inhibition of zinc by benzotriazole with an electrochemical quartz crystal microbalance.* Journal of The Electrochemical Society, 2003. **150**(4): p. B176-B180.
35. N. LeBozec, D. Thierry, A. Peltola, L. Luxem, G. Luckeneder, G. Marchiaro, M. Rohwerder, *Corrosion performance of Zn–Mg–Al coated steel in accelerated corrosion tests used in the automotive industry and field exposures.* Materials and Corrosion, 2013. **64**: p. 969-978.
36. M. Salgueiro Azevedo, C. Allély, K. Ogle, P. Volovitch, *Corrosion mechanisms of Zn(Mg,Al) coated steel: the effect of HCO3− and NH4+ ions on the intrinsic reactivity of the coating.* Electrochimica Acta, 2015. **153**: p. 159-169.
37. F. Rosalbino, E. Angelini, D. Macciò, A. Saccone, S. Delfino, *Application of EIS to assess the effect of rare earths small addition on the corrosion behaviour of Zn–5% Al (Galfan) alloy in neutral aerated sodium chloride solution.* Electrochimica Acta, 2009. **54**: p. 1204-1209.
38. N. Kovačević, A. Kokalj, *Chemistry of the interaction between azole type corrosion inhibitor molecules and metal surfaces.* Materials Chemistry and Physics, 2012. **137**(1): p. 331-339.
39. K. Xhanari, M. Finšgar, *Organic corrosion inhibitors for aluminum and its alloys in chloride and alkaline solutions: A review.* Arabian Journal of Chemistry, 2019. **12**(8): p. 4646-4663.
40. T. J. Harvey, F. C. Walsh, A. H. Nahlé, *A review of inhibitors for the corrosion of transition metals in aqueous acids.* Journal of Molecular Liquids, 2018. **266**: p. 160-175.
41. G. Williams, H. N. Mcmurray, *Inhibition of filiform corrosion on organic-coated AA2024-T3 by smart-release cation and anion-exchange pigments.* Electrochimica Acta, 2012. **69**: p. 287-294.
42. G. Markevicius, S. Chaudhuri, C. Bajracharya, R. Rastogi, J. Xiao, C. Burnett, T. Q. Chastek, *Polyoligomeric silsesquioxane (POSS)–hydrogenated polybutadiene polyurethane coatings for corrosion inhibition of AA2024.* Progress in Organic Coatings, 2012. **75**: p. 319-327.
43. M. Serdechnova, A. N. Salak, F. S .Barbosa, D. E. L. Vieira, J.Tedim, M. L. Zheludkevich, M. G. S.Ferreira, *Interlayer intercalation and arrangement of 2-mercaptobenzothiazolate and 1,2,3-*

benzotriazolate anions in layered double hydroxides: In situ X-ray diffraction study. Journal of Solid State Chemistry, 2016. **233**: p. 158-165.
44. C. A. J. Richards, H. N. McMurray, G. Williams, *Smart-release inhibition of corrosion driven organic coating failure on zinc by cationic benzotriazole based pigments.* Corrosion Science, 2019. **154**: p. 101-110.
45. S. Sheikholeslami, *Long-Term Field-Performance of Waterborne Coatings*, in *Department of Chemical and Materials Engineering*. 2021, The University of Auckland: New Zealand.
46. G. Williams, H. N. McMurray, *Localized Corrosion of Magnesium in Chloride-Containing Electrolyte Studied by a Scanning Vibrating Electrode Technique.* Journal of The Electrochemical Society, 2008. **155**(7): p. C340-C349.
47. G. Williams, H. N. McMurray, R.Grace, *Inhibition of magnesium localised corrosion in chloride containing electrolyte.* Electrochimica Acta, 2010. **55**(27): p. 7824-7833.
48. N. Wint, Z. S. Barrett, G. Williams, H. N. McMurray, *The Study of AA2024 De-Alloying Using Luminol Electrogenerated Chemiluminescence Imaging.* Journal of The Electrochemical Society, 2019. **166**(11): p. C3417-C3430.
49. A. S. Gnedenkov, D. Mei, S. V. Lamaka, S. L. Sinebryukhov, D. V. Mashtalyar, I. E. Vyaliy, M. L. Zheludkevich, S. V. Gnedenkov, *Localized currents and pH distribution studied during corrosion of MA8 Mg alloy in the cell culture medium.* Corrosion Science, 2020. **170**: p. 108689.
50. L. M. Calado, M. G. Taryba, Y. Morozov, M. J. Carmezim, M. F. Montemor, *Novel smart and self-healing cerium phosphate-based corrosion inhibitor for AZ31 magnesium alloy.* Corrosion Science, 2020. **170**: p. 108648.
51. A. S. Gnedenkov, S. L. Sinebryukhov, D. V. Mashtalyar, S. V. Gnedenkov, *Localized corrosion of the Mg alloys with inhibitor-containing coatings: SVET and SIET studies.* Corrosion Science, 2016. **102**: p. 269-278.
52. M. Mouanga, F. Andreatta, M. E. Druart, E. Marin, L. Fedrizzi, M. G. Olivier, *A localized approach to study the effect of cerium salts as cathodic inhibitor on iron/aluminum galvanic coupling.* Corrosion Science, 2015. **90**: p. 491-502.
53. J. W. Lee, B. R. Park, S. Y. Oh, D. W. Yun, J. K. Hwang, M. S. Oh, S. J. Kim, *Mechanistic study on the cut-edge corrosion behaviors of Zn-Al-Mg alloy coated steel sheets in chloride containing environments.* Corrosion Science, 2019. **160**: p. 108170.
54. A. G. Marques, J. Izquierdo, R. M. Souto, A. M. Simões, *SECM imaging of the cut edge corrosion of galvanized steel as a function of pH.* Electrochimica Acta, 2015. **153**: p. 238-245.